MiR-202-3p inhibits the proliferation and metastasis of lung adenocarcinoma cells by targeting RRM2

Xiaowen Cao[1#], Fangsu Xue[2#], Haoyu Chen[1], Lu Shen[1], Xiaosa Yuan[1], Yunchi Yu[1], Ying Zong[3], Lou Zhong[1], Fang Huang[4]

[1]Department of Thoracic Surgery, Affiliated Hospital of Nantong University, Nantong, China; [2]Department of Respiration, Binhai County People's Hospital, Yancheng, China; [3]Medical College of Nantong University, Nantong, China; [4]Department of Pathology, Affiliated Hospital of Nantong University, Nantong, China

Contributions: (I) Conception and design: L Zhong; (II) Administrative support: L Zhong; (III) Provision of study materials or patients: X Cao, H Chen, L Shen, Y Yu, X Yuan; (IV) Collection and assembly of data: X Cao, H Chen, X Yuan, F Huang, L Zhong; (V) Data analysis and interpretation: L Zhong, F Xue; (VI) Manuscript writing: All authors; (VII) Final approval of the manuscript: All authors.

[#]These authors contributed equally to this work.

Correspondence to: Prof. Lou Zhong. Department of Thoracic Surgery, Affiliated Hospital of Nantong University, Nantong 226001, China. Email: zhongl80@126.com; Fang Huang. Department of Pathology, Affiliated Hospital of Nantong University, Nantong 226001, China. Email: 1742752687@qq.com.

Background: Lung adenocarcinoma (LUAD) is the most common type of lung cancer, and its pathogenesis is still unclear. The present study aimed to investigate the role of *miR-202-3p* and its downstream target gene, ribonucleotide reductase regulatory subunit M2 (*RRM2*), in the occurrence and development of LUAD and elucidate the correlation between *RRM2* and the clinicopathological stage and prognosis of LUAD.

Methods: The expression of *miR-202-3p* was analyzed using the CancerMIRNome database and quantitative polymerase chain reaction (qPCR). The effects of *miR-202-3p* and *RRM2* on the proliferation, migration, and invasion of A549 cells were analyzed. A dual luciferase reporter assay was used to verify the targeting of *miR-202-3p* and *RRM2*. Additionally, the correlation between *RRM2* expression and clinicopathology was analyzed.

Results: (I) *MiR-202-3p* was lowly expressed in LUAD and the LUAD cell lines. qPCR confirmed that microRNA (miRNA) transfection was effective and sufficient for subsequent experiments. (II) *MiR-202-3p* inhibited the proliferation, invasion, and migration of LUAD cells. (III) There was a targeting relationship between *miR-202-3p* and *RRM2*, and *miR-202-3p* affected the expression of the *RRM2* protein. *RRM2* was highly expressed in lung cancer tissue. (IV) *RRM2* was associated with the clinicopathological staging of lung cancer. The prognosis of patients with low *RRM2* expression was better, and the prognostic sensitivity of *RRM2* to lung cancer was high. *RRM2* may exert its effects via the Notch pathway. (V) Si-*RRM2* inhibited the expression of the *RRM2* protein. *RRM2* promoted the proliferation, migration, and invasion of LUAD cells. A *miR-202-3p* inhibitor restored the inhibitory effect of si-*RRM2* on LUAD cells.

Conclusions: *MiR-202-3p* was lowly expressed in lung cancer tissue. *MiR-202-3p* overexpression inhibited the proliferation and metastasis of lung cancer cells. *RRM2* was highly expressed in lung cancer tissue and promoted the proliferation and metastasis of lung cancer cells. *MiR-202-3p* targeted and inhibited *RRM2*, thereby reducing the proliferation and metastasis of LUAD cells. LUAD patients with low *RRM2* expression had a better prognosis, and the expression level of *RRM2* was correlated with the clinical characteristics of lung cancer patients.

Keywords: Lung adenocarcinoma (LUAD); *miR-202-3p*; ribonucleotide reductase regulatory subunit M2 (*RRM2*); metastasis; proliferation

Submitted Oct 18, 2022. Accepted for publication Dec 20, 2022.
doi: 10.21037/atm-22-6089
View this article at: https://dx.doi.org/10.21037/atm-22-6089

Introduction

Lung cancer (LC) has the highest incidence among all malignancies worldwide and is also the most common cause of cancer-related death (1,2). LC can be divided into small cell lung cancer (SCLC) and non-small cell lung cancer (NSCLC) based on its histology and etiology. In China, the incidence of NSCLC accounts for approximately 85% of LC cases, and its histology is usually dominated by adenocarcinoma and squamous cell carcinoma (3).

Lung adenocarcinoma (LUAD) is currently the most common histological subtype of primary LC, accounting for approximately 40% of LC cases, and the relative incidence of LUAD is still increasing (4,5). The prognosis of patients with various tissue subtypes of LUAD is very poor (6). Although there have been considerable advancements in treatment strategies for LUAD, the overall short-term survival of NSCLC patients has not exceeded 20% in the past few decades (3). Increasing evidence indicates that malignant proliferation and distant metastasis are the main challenges of cancer treatment (7). Therefore, studying the genes associated with tumor metastasis in the pathophysiological process of LUAD is crucial, and targeting these genes may be a potential approach for the treatment of NSCLC. Although a large number of studies have been carried out on LC, the molecular regulatory mechanisms of the occurrence and development of LC have not been systematically investigated.

MiRNA, the most abundant small RNA, are one of the most abundant gene regulatory molecules and can affect the output of several protein-coding genes in multicellular organisms. They are a class of small non-coding RNAs that are highly conserved in evolution, with a length of approximately 19–22 nucleotides (nt). Mature miRNAs, as posttranscriptional inhibitors, recognize and bind to the 3' untranslated region (3'UTR) of target genes through complete or incomplete complementary pairing, thereby destabilizing target mRNAs and inhibiting the translation of target genes. MiRNAs play important regulatory roles in both animals and plants. An increasing number of studies have shown that miRNAs are extensively involved in basic cellular biological processes, such as cell differentiation, proliferation, growth, migration, and apoptosis, as well as carcinogenic or cancer-inhibiting processes (8-10).

MiR-202-3p is present in many human diseases and is a new potential biomarker for the diagnosis of type 1 gastric neuroendocrine tumors (11). Its overexpression in bone marrow mesenchymal stem cells improves cerebral ischemia-reperfusion injury by promoting angiogenesis and inhibiting inflammation (12). Additionally, the overexpression of nuclear-enriched autosomal transcript 1 promotes the proliferation, migration, and invasion of endometrial cancer cells and inhibits apoptosis by targeting the *miRNA-202-3p*/T-cell immunoglobulin and mucin domain 4 axis (13). However, the pathophysiological role of *miR-202-3p* in NSCLC is not completely clear.

Ribonucleotide reductase (RR) is the only rate-limiting enzyme in intracellular DNA synthesis and plays an important role in nucleic acid metabolism. It can catalyze the reduction of nucleoside diphosphate to deoxyribonucleoside diphosphate, which is the rate-limiting step in the biosynthesis of deoxyribonucleoside triphosphate (dNTP) (14). RR includes two subunits, M1 and M2, both of which are dimeric structures. The ribonucleotide reductase regulatory subunit M2 (*RRM2*) has a site that binds to substrates and allosteric effectors and contains a direct electron-donating group, such as a sulfhydryl, controlling the substrate specificity and enzyme activity and acting as a tumor suppressor gene. *RRM2* is an iron-sulfur protein that participates in catalytic reactions through the formation of specific free radicals through the benzene ring of tyrosine residues. *RRM2* is not only the catalytic region responsible for substrate conversion but also carries the contact inhibition region and is the main regulatory element of RR activity (15).

Highlight box

Key findings

- MiR-202-3p inhibited the proliferation and metastasis of lung cancer cells by targeting RRM2. LUAD patients with high miR-202-3p or low RRM2 expression had a better prognosis.

What is known and what is new?

- MiR-202-3p was lowly expressed in lung cancer tissue. MiR-202-3p overexpression inhibited the proliferation and metastasis of lung cancer cells. RRM2 was highly expressed in lung cancer tissue and promoted the proliferation and metastasis of lung cancer cells;
- MiR-202-3p targeted and inhibited RRM2, thereby reducing the proliferation and metastasis of LUAD cells. LUAD patients with low RRM2 expression had a better prognosis, and the expression level of RRM2 was correlated with the clinical characteristics of lung cancer patients.

What is the implication, and what should change now?

- Our findings not only further enrich the molecular mechanism of lung cancer development and progression, but also provide a molecular basis for targeted treatment of lung cancer.

RRM2 is involved in the biosynthesis of dNTP and is an indispensable key enzyme in the process of DNA synthesis and repair. Wang *et al.* used a mouse xenograft model to confirm that *RRM2* activates the extracellular regulated protein kinases 1/2 (ERK1/2) pathway through reactive oxygen species (ROS) proto-oncogene 1-receptor tyrosine kinase to promote the formation of blood vessels in cervical cancer cells, increases microvessel density, and promotes the proliferation of tumor cells (16). Research has indicated that *RRM2* overexpression increases the invasiveness of pancreatic cancer by enhancing the expression of matrix metallopeptidase 9 (MMP-9) (17). Rasmussen *et al.* showed that *RRM2* affects the upstream tumor suppressor gene *BRCA1* to form the *BRCA1-RRM2* axis, protecting glioblastoma (GBM) cells from interference by endogenous apoptotic factors such as oncogenes and DNA damage, resulting in GBM invasion and metastasis (18). Wang *et al.* found that silencing *RRM2* inhibits the proliferation, invasion, and migration of GBM cells and increases the rate of apoptosis. *RRM2* overexpression promotes cell proliferation, migration, and invasion and inhibits cell apoptosis (19). *In vivo*, *RRM2* overexpression was shown to accelerate the growth of GBM cells; in the study, *RRM2* was highly expressed in human GBM cells. *RRM2* promotes the proliferation, migration, and invasion of human GBM cells but inhibits cell apoptosis. In recent years, *RRM2* has been shown to be overexpressed in a variety of malignant tumors, such as brain GBM, cholangiocarcinoma, pancreatic cancer, breast cancer, NSCLC, ovarian cancer, bladder cancer, and colorectal cancer (20-23). Therefore, studies on the effects of abnormal *RRM2* expression on the proliferation, chemotherapy resistance, and metastasis of malignant tumors and the prognosis and survival of patients with such tumors can provide a new theoretical basis for the diagnosis, treatment, and prognosis of clinical malignant tumors. We present the following article in accordance with the MDAR reporting checklist (available at https://atm.amegroups.com/article/view/10.21037/atm-22-6089/rc).

Methods

Data

In this study, the mRNA expression data of 594 LUAD transcriptomes were downloaded from The Cancer Genome Atlas (TCGA) database (https://tcga-data.nci.nih.gov/tcga/), and the expression data were sorted and extracted using Perl; a total of 59 normal samples and 535 tumor samples were included. TCGA database was used to obtain the clinical data of 522 LUAD patients, from which survival time, survival status, sex, age, TNM stage, and clinicopathological stage were extracted through Perl. Some clinical characteristic data were incomplete. Cases with unknown data were excluded from the analysis. The study was conducted in accordance with the Declaration of Helsinki (as revised in 2013).

RRM2 survival was analyzed using the survival package in R language. The matrix/immune score was used to divide the samples into high and low groups using the median score as the boundary. A survival curve was plotted using the Kaplan-Meier (K-M) method. The clinicopathological staging data were sorted, and unknown samples were then removed before correlation analysis. Each object in the results was analyzed by paired comparison to obtain the P values.

The differential analysis of gene profiles was performed using the limma package in R language. Differentially expressed genes (DEGs) were screened using $|\log_2(\text{fold change})| > 1$ and $-\log_{10}(\text{P value}) < 0.05$ to obtain the upregulated and downregulated gene sets. Next, a volcano plot was constructed. A heatmap was then plotted using the pheatmap package in R language, and 20 upregulated and 20 downregulated genes were presented according to their $|\log_2(\text{fold change})|$ value. Finally, the VennDiagram package in R was used to draw a Venn diagram to obtain the genes related to *miR-202-3p* in the miRTarBase, MiRDB, and TargetScan databases. These genes and the above DEGs were used to determine the function of the DEGs. To discover the function of the DEGs, we conducted Gene Ontology (GO) and Kyoto Encyclopedia of Genes and Genomes (KEGG) enrichment analysis and plotted the enrichment pathway results using the ggplot2 package in R language.

Univariate Cox regression analysis of the clinical prognostic data of *RRM2* was performed using the survival package in R language. A Cox risk model was built using R language, and a coefficient was obtained for each gene. The risk score was equal to the sum of the expression level of each gene multiplied by the coefficient, and the model was optimized. First, the survival analysis method described above was used to draw a survival curve of the risk model and a risk curve. The risk model and clinical characteristics and survival prognosis were then subjected to Cox regression analysis, and the results were viewed using forest plots. Next, the survivalROC package in R was

used to plot the receiver operating characteristic (ROC) curves for the risk model and clinical characteristics. Finally, the correlation between the risk model and clinical characteristics was analyzed.

Cells and main reagents

A549, H1975, human NSCLC cells, and Beas-2b normal bronchial epithelial cells were purchased from Guangzhou Cellcook Biotechnology Co., Ltd. (China). Fetal bovine serum (FBS), RPMI-1640 medium, and Dulbecco's Modified Eagle Medium (DMEM) were purchased from Biological Industries (BioInd, Israel). Ham's F-12K medium was purchased from Gibco (USA), and TRIzol reagent was purchased from Nanjing Vazyme Biotech Co. (China). The miRNA mimic/inhibitor/control were purchased from Guangzhou RibPharm Co., Ltd. (China), trypsin-ethylene diamine tetraacetic acid (EDTA) was purchased from New Cell & Molecular Biotech Co., Ltd. (Suzhou, China), JetPrime transfection reagent was purchased from Polyplus Co., Ltd. (France), and ChamQ Universal SYBR quantitative polymerase chain reaction(qPCR) Master Mix reagent and HiScript III All-in-one RT SuperMix Perfect for qPCR were purchased from Nanjing Vazyme Biotech Co., Ltd. The *RRM2* (ab57653) and β-actin (ab8226) antibodies were purchased from Abcam (USA), and the goat anti-mouse secondary antibody and goat anti-rabbit secondary antibody were purchased from Shanghai Beyotime Biotechnology (China). The Cell Counting Kit-8 (CCK-8) reagent was purchased from Tongren Company (Japan), and small interfering RNA (siRNA) was purchased from Suzhou GenePharma Co., Ltd. (China).

Cell culture

The A549 and H1975 human LUAD cell lines and human normal bronchial epithelial cell line Beas-2b were selected for culture. A549 cells were cultured in F-12k medium, H1975 cells were cultured in RPMI-1640 medium, and Beas-2b cells were cultured in DMEM. The above medium was supplemented with 10% FBS and 1% penicillin-streptomycin. The cells were cultured in a 37 ℃ incubator with 5% carbon dioxide (CO_2). The medium was changed every other day, and the original medium was discarded when changing the medium. The plates were rinsed with phosphate-buffered saline (PBS) three times; to avoid contamination, all PBS was aspirated after each rinse, after which fresh medium was added. The growth of the cells was observed using a microscope, and a growth curve was plotted. When the cells were in the logarithmic growth phase, 0.5–1 mL of trypsin digestion solution containing 0.25% EDTA was added, and the cells were placed in a 37 ℃, 5% CO_2 incubator for 2 min.

The state of the cells was observed under a microscope (NIKON, Japanese). When the cells became round with an increase in intercellular gaps, 3 mL of the complete medium containing 10% FBS was added to terminate the digestion, and the cells that were still adherent were pipetted into the cell suspension. Next, the cell suspension was placed in a centrifuge tube and centrifuged at 1,000 rpm for 5 min. The supernatant was then discarded, the cell pellet was resuspended, and a new medium containing 10% FBS was added. The cells were passaged every 2–3 days. Cells in the logarithmic growth phase were used in all experiments.

Cell transfection

Oligonucleotides were synthesized by RiboBio Co., Ltd. (RiboBio, Guangzhou, China). SiRNA was provided by GenePharma (Suzhou, China). The cells were divided into a scrambled group, a *miR-202-3p* mock group, a *miR-202-3p* inhibitor group, a si-*RRM2* negative control (NC) group, a *miR-202-3p* inhibitor + *RRM2* siRNA group, and a *RRM2* siRNA group. Cells in the logarithmic growth phase (2.0×10^6 cells/well) were cultured in six-well plates without antibiotics for 24 h before transfection. When the cells were 80% confluent, 50 nM *miR-202-3p* NC, 20 nM *miR-202-3p* mimics, 100 nM *miR-202-3p* inhibitor, 100 nM si-NC, and 100 nM *miR-202-3p* inhibitor + *RRM2* siRNA or 100 nM *RRM2* siRNA were transfected using polyplus JetPrime. Forty-eight hours after transfection, the cells were collected for subsequent experiments.

Analysis of dual luciferase reporter genes

The Promega Dual-Luciferase system 1.5× passive lysis buffer (PLB) was diluted with distilled water to 1× PLB, 100 μL of PBS was added to each well of a 96-well plate, and the cells were dispersed by pipetting. The plates were placed on a shaker at room temperature. After shaking for 15 min, the cell lysate was aspirated into a 1.5 mL centrifuge tube, and the lysate was centrifuged at 12,000 rpm at 4 ℃ for 10 min. The supernatant was then transferred to a new tube.

Next, 100 μL of Luciferase Assay Reagent II [Luciferase

Assay Reagent, Promega (Madison, WI, USA)] was added to each well of the 96-well plate and 20 µL of cell lysate was also added, followed by mixing by pipetting 2–3 times. The firefly luciferase value was then measured and recorded, serving as the internal reference value. Subsequently, 100 µL of Stop & Glo® Reagent (Luciferase Assay Reagent, Promega) was added, followed by mixing by pipetting 2–3 times. The Renilla luciferase value was then measured and recorded, serving as the luminescence value for the reporter gene.

Transwell migration experiment

Cell migration experiments were performed in 24-well plates (Corning, New York, USA). A549 cells (2.5×10^5 cells/well) were seeded into the culture medium without FBS in the upper chamber, and a complete culture medium containing 10% FBS was added to the lower chamber. After 24 h, the cells that migrated to the lower surface of the filter were fixed with 4% paraformaldehyde (PFA) and incubated with 4',6-Diamidino-2'-phenylindole (DAPI, 1:1,000, Invitrogen, CA, USA) at room temperature for 5 min. Migrated cells were counted in five random areas under an inverted fluorescence microscope (Leica DMI6000B, Wetzlar, Germany). All experiments were performed in triplicate.

Real-time polymerase chain reaction (RT-PCR)

Reverse transcription was performed using HiScript III RT SuperMix for qPCR (Nanjing Vazyme Biotech Co., Ltd.). RT-PCR was performed using the ChamQ Universal SYBR qPCR Master Mix kit (Nanjing Vazyme Biotech Co., Ltd.) and a Thermo Fisher StepOne (USA) RT-PCR system. U6 and glyceraldehyde-3-phosphate dehydrogenase (GAPDH) were used as internal controls. The reverse primer sequence for U6 was 5'-AACGCTTCACGAATTTGCGT-3', and the forward primer sequence was 5'-CTCGCTTCGGCAGCACA-3'; the reverse primer sequence for GAPDH was 5'-GGAGCG AGATCCCTCCAAAAT-3', and the forward primer sequence was 5'-GGCTGTTGTCATACT TCTCATGG-3'; the forward primer sequence for *RRM2* was 5'-TTGAAACGATGCCTTGTGTCA-3', and the reverse sequence was 5'-ACCATAGGTAGCC TCTTTGTCC-3'; and the primers for *miR-202-3p* were Bulge-loop™ miRNA qRT-PCR Primer Sets (one RT primer and a pair of qPCR primers for each set) specific to miR-202-3p and designed by RiboBio (Guangzhou, China). All experiments were repeated three times. The qPCR conditions for *RRM2* were as follows: predenaturation at 95 ℃ for 30 s; amplification (40 cycles) at 95 ℃ for 10 s and 60 ℃ for 30 s; and 95 ℃ for 15 s, 60 ℃ for 60 s, and 95 ℃ for 15 s. The relative expression level of the target gene was calculated using the $2^{-\Delta\Delta Ct}$ method. The qPCR conditions for *miR-202-3p* were as follows: predenaturation at 95 ℃; amplification at 95 ℃ for 2 s, 60 ℃ for 20 s, and 70 ℃ for 10 s; and 95 ℃ for 15 s, 60 ℃ for 60 s, and 95 ℃ for 15 s. The relative expression level of the target gene was calculated using the $2^{-\Delta\Delta Ct}$ method.

CCK-8 test

CCK-8 (Dojindo, Kumamoto, Japan) was used according to the manufacturer's instructions. A549 cells were seeded in 96-well plates (3×10^3 cells/well) and cultured overnight. The absorbance at 450 nm was measured using a microplate reader (Shanghai, Thermo Fisher Science, Shanghai, China) for 4 consecutive days. This experiment was repeated three times independently.

Western blot (immunoblot)

Cells were collected and lysed in Radio-Immunoprecipitation Assay (RIPA) lysis buffer containing protease inhibitors. After centrifugation, the supernatant was mixed with dithiothreitol (DTT)/2× sodium dodecyl sulfate (SDS) loading buffer and boiled in water. Then total proteins were separated by SDS-polyacrylamide gel electrophoresis (PAGE), and transferred to polyvinylidene fluoride (PVDF) membranes. The PVDF membrane was immersed in a blocking solution [5% bovine serum albumin (BSA) dissolved in PBST (PBS pH 7.5, 0.1% Tween 20)] for 1 h at room temperature. The membrane was washed with PBST, incubated with primary antibody [rabbit anti-human *RRM2* antibody (1:1,000) and mouse anti-human β-actin antibody (1:1,000)] at 4 ℃ overnight, and washed again with PBST for three times. The membranes were incubated at room temperature with the appropriate secondary antibodies [horseradish peroxidase (HRP)-conjugated goat anti-rabbit secondary antibody (1:1,000) and HRP-conjugated goat anti-mouse secondary antibody (1:1,000)] for 1 h and rinsed with PBST for three times. Chemiluminescence detection system (Bio Rad Laboratories, Hercules, USA) was used to detect gray stripe. Image J software was used to analyze the grayscale of the strips.

Statistical analysis

In this study, R language was used to perform the statistical analyses. The Wilcoxon rank sum test was employed to screen the genes. Significance tests were applied for the correlations. One-way analysis of variance and *t*-tests were utilized to detect differences. Univariate and multivariate Cox analyses and the construction of the Cox models were performed using R language. All experiments were repeated three times independently, and the data were expressed as the mean ± standard deviation (SD). The independent sample *t*-test was used to compare the means of unpaired groups. The figures were created in R language and GraphPad Prism 8 (GraphPad Software, San Diego, CA).

Results

Expression of miR-202-3p in various tumor tissues and ROC analysis

The expression level of *miR-202-3p* in various tumors was analyzed using CancerMIRNome. The expression of *miR-202-3p* in LUAD was low (P<0.05) (*Figure 1A*), and the area under the ROC curve (AUC) for LUAD was 0.77 (P<0.05). This finding indicates that *miR-202-3p* has a high sensitivity in the diagnosis of LUAD (*Figure 1B*,*1C*).

Changes in miR-202-3p expression in NSCLC

The analysis of CancerMIRNome indicated that the expression of *miR-202-3p* was low in LUAD tissue, P<0.05 (*Figure 2A*), which was also confirmed by qPCR in Beas-2b, A549, and H1975 cells, i.e., the expression of *miR-202-3p* was higher in the normal epithelial cells than in the LC cell lines (*Figure 2B*).

Detection of miR-202-3p expression in A549 cells after transfection

The *miR-202-3p* mimics, *miR-202-3p* inhibitor, and miR-NC were transfected into A549 cells. Forty-eight hours after transfection, the expression level of *miR-202-3p* was detected by qPCR. The results showed that compared with that in the miR-NC group, the expression level of *miR-202-3p* in the mimic group was significantly higher than that in the miR-NC group and that in the inhibitor group was lower than that in the miR-NC group (P<0.05, *Figure 3*).

MiR-202-3p inhibits the proliferation of LUAD cells

The effects of *miR-202-3p* and *RRM2* on the proliferation of A549 cells were examined using CCK-8 assays. The results showed that the growth rate of the *miR-202-3p* mimics group was lower than that in the NC group 48 h after transfection. In contrast, the growth rate of the *miR-202-3p* inhibitor group was significantly higher than that of the NC group (*Figure 4*), indicating that *miR-202-3p* inhibits the proliferation of LUAD cells.

MiR-202-3p inhibits the migration of LUAD cells

The effect of *miR-202-3p* on the migration ability of A549 cells was detected using the Transwell method. The results of the migration and invasion experiments indicated that the *miR-202-3p* inhibitor group had the most cells pass through the Transwell membrane, followed by the *miR-202-3p* NC group and the *miR-202-3p* mimics group, which had the fewest cells pass through the membrane (*Figure 5*). Therefore, it can be concluded that *miR-202-3p* inhibits the migration and invasion of LUAD cells.

Prediction of miR-202-3p-related genes

We performed bioinformatics analysis of NSCLC using TCGA, which is a public gene expression dataset. Next, the DEGs between the tumor and normal samples were identified using the Wilcoxon rank sum test. The DEGs associated with *miR-202-3p* were identified and divided into high- and low-expression groups (*Figure 6A*). Cluster analysis of the DEGs revealed 20 upregulated genes and 20 downregulated genes (*Figure 6B*). A comparison of the three databases (i.e., mRDB, miRTarBase, and TargetScan) showed that among the predicted genes related to *miR-202-3p*, 75 genes intersected in the three databases (*Figure 6C*). Moreover, comparing the target mRNAs and the upregulated DEGs, 29 genes intersected (*Figure 6D*).

Subsequent univariate Cox proportional hazard regression analysis of these genes showed that *RRM2* and leucine rich repeat and fibronectin type III domain containing 4 (LRFN4) were related to clinical prognosis (*Figure 6E*). Based on a previous study on *RRM2* in LC, the role of *RRM2* in LC is more important than that of LRFN4 (24). Thus, the *RRM2* gene was selected for further study. Analysis of the CancerMIRNome database showed that *miR-202-*

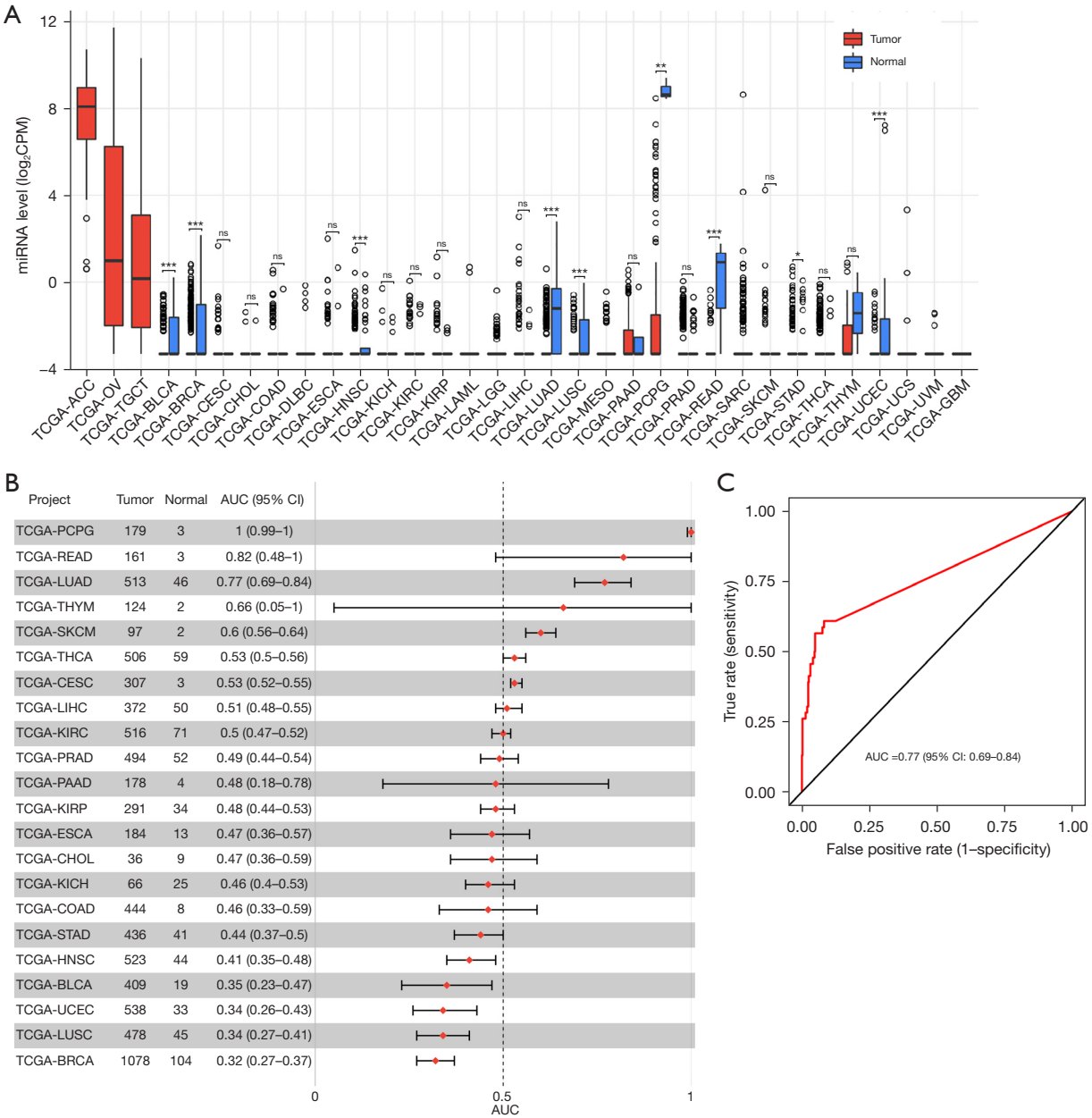

Figure 1 *MiR-202-3p* expression level and ROC analysis in a variety of tumors. (A) The expression of *miR-202-3p* was low in LUAD, P<0.05. (B) AUC values for *miR-202-3p* in multiple groups of tumors. (C) ROC curve for *miR-202-3p* in LUAD. *, P<0.05; **, P<0.01; ***, P<0.001. ACC, adrenocortical carcinoma; AUC, area under the curve; BLCA, bladder urothelial carcinoma; BRCA, breast invasive carcinoma; CESC, cervical squamous cell carcinoma and endocervical adenocarcinoma; CHOL, cholangiocarcinoma; CI, confidence interval; COAD, colon adenocarcinoma; CPM, clique percolation method; DLBC, lymphoid neoplasm diffuse large B-cell lymphoma; ESCA, esophageal carcinoma; GBM, glioblastoma; HNSC, head and neck squamous cell carcinoma; KICH, kidney chromophobe; KIRC, kidney renal clear cell carcinoma; KIRP, kidney renal papillary cell carcinoma; LAML, acute myeloid leukemia; LGG, brain lower grade glioma; LIHC, liver hepatocellular carcinoma; LUAD, lung adenocarcinoma; LUSC, lung squamous cell carcinoma; MESO, mesothelioma; ns, not significant; OV, ovarian serous cystadenocarcinoma; PAAD, pancreatic adenocarcinoma; PCPG, pheochromocytoma and paraganglioma; PRAD, prostate adenocarcinoma; READ, rectum adenocarcinoma; ROC, receiver operating characteristic; SARC, sarcoma; SKCM, skin cutaneous melanoma; STAD, stomach adenocarcinoma; TGCT, testicular germ cell tumors; THCA, thyroid carcinoma; THYM, thymoma; UCEC, uterine corpus endometrial carcinoma; UCS, uterine carcinosarcoma; UVM, uveal melanoma.

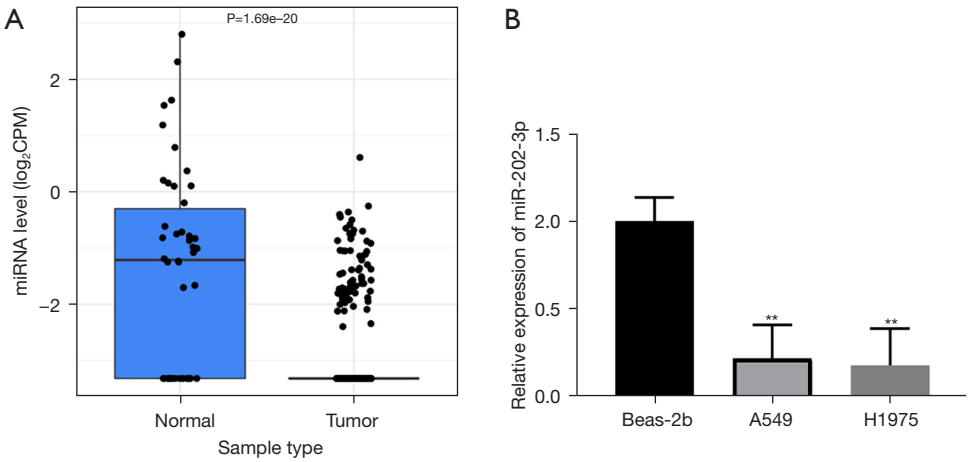

Figure 2 Expression of *miR-202-3p* in NSCLC. (A) CancerMIRNome data analysis showed that the expression level of *miR-202-3p* in the lung tumor tissue was lower than that in the normal tissue. (B) The expression of *miR-202-3p* in Beas-2b cells was higher than that in A549 and H1975 cells. The P value was calculated using a parametric test: **, P<0.01. CPM, clique percolation method; NSCLC, non-small cell lung cancer.

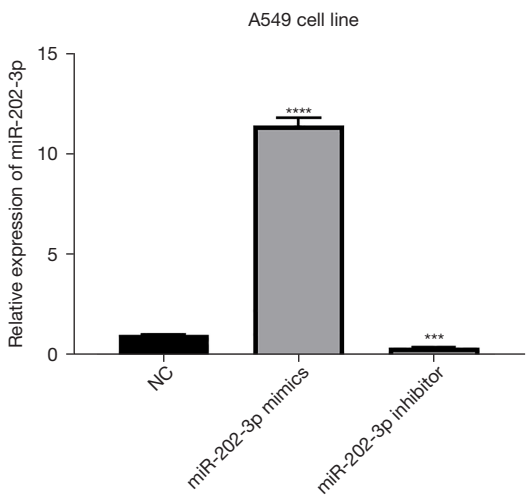

Figure 3 qPCR detection of the expression levels of *miR-202-3p* in cells after transfection. The mimics, inhibitor, and miR-NC groups were compared, and the P values were calculated using parametric tests. ***, P<0.001; ****, P<0.0001. NC, negative control; qPCR, quantitative PCR.

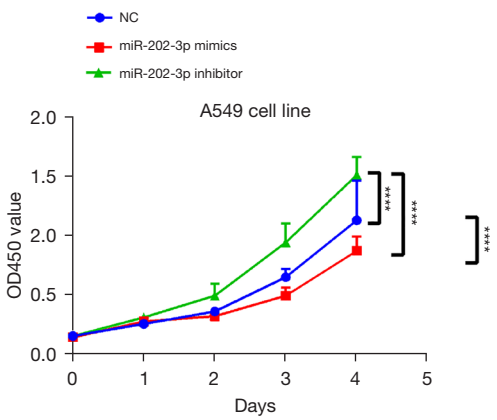

Figure 4 *MiR-202-3p* inhibits the proliferation of NSCLC cells. The results of the CCK-8 assays indicate that the A549 cells in the miR-202-3p mimics group showed the slowest growth, followed by the miR-NC group and the *miR-202-3p* inhibitor group, which exhibited the fastest growth. The P value was calculated using a parametric test: ****, P<0.0001. CCK-8, Cell Counting Kit 8; NC, negative control; NSCLC, non-small cell lung cancer; OD, optical density.

3p was negatively correlated with *RRM2* expression, with a correlation coefficient of R=–0.296, P<0.05 (*Figure 6F*).

Expression of RRM2 in LC cells

TCGA database also showed that *RRM2* was highly expressed in LC tissue (*Figure 7A*). qPCR confirmed that the relative expression of *RRM2* in Beas-2b normal tracheal epithelial cells was lower than that in the LC cell lines (*Figure 7B*).

MiR-202-3p directly targets RRM2

We also constructed a luciferase reporter vector to analyze

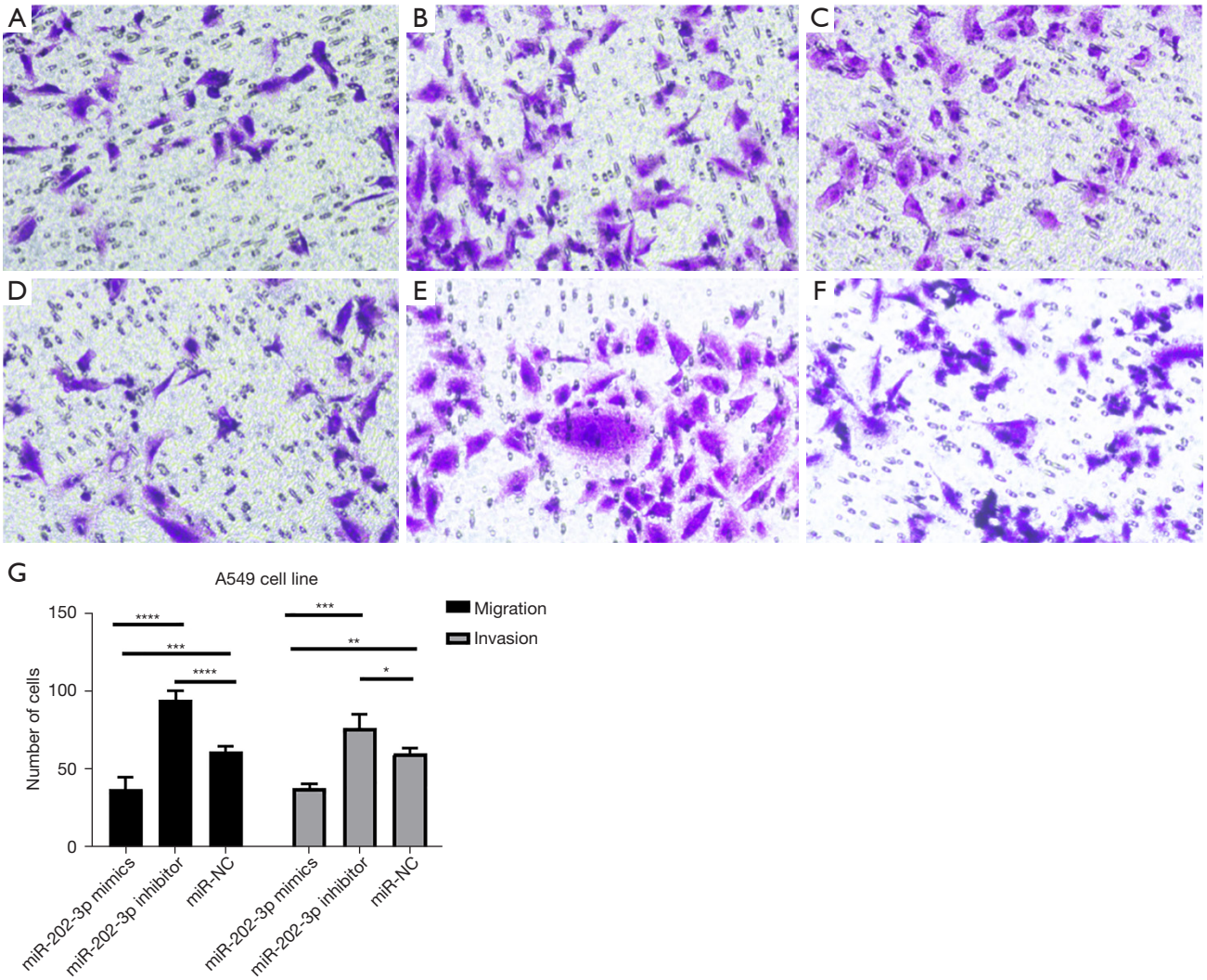

Figure 5 Transwell experiment to test the migration and invasion ability of each group of cells. A549 cells were used in the Transwell experiments (crystal violet staining). (A) Migration experiment for the *miR-202-3p* mimics group; (B) migration experiment for the *miR-202-3p* inhibitor group; (C) migration experiment for the miR-NC group; (D) invasion experiment for the *miR-202-3p* mimics group; (E) invasion experiment for the *miR-202-3p* inhibitor group; (F) invasion experiment for the miR-NC group; (G) the number of migratory and invasive cells in the Transwell. Intergroup comparisons were performed. P values were calculated using parametric tests. *, P<0.05; **, P<0.01; ***, P<0.001; ****, P<0.0001. Original magnification was ×200 for A-F.

dual luciferase reporter genes. The binding of *miR-202-3p* to the h-RRM2-3UTR is shown in *Figure 8A*. The dual luciferase reporter gene analysis of H293T cells confirmed that *RRM2* contains a direct binding site for *miR-202-3p*. As shown in *Figure 8B*, following transfection of the *miR-202-3p* mimics, the luciferase activity in the h-RRM2-3UTR-wild type (wt) group was significantly decreased, while that in the h-RRM2-3UTR-mutant (mu) group did not change. These results confirmed that *miR-202-3p* directly targets the *RRM2* gene.

Western blot assays were used to detect the expression of the *RRM2* protein after transfection, and the results are shown in *Figure 8C*. Compared with that in the *miR-NC* group, the expression of the *RRM2* protein was higher in the *miR-202-3p* inhibitor group, and the expression of the *RRM2* protein in the *miR-202-3p* mimics group was markedly lower; the difference was statistically significant (P<0.05).

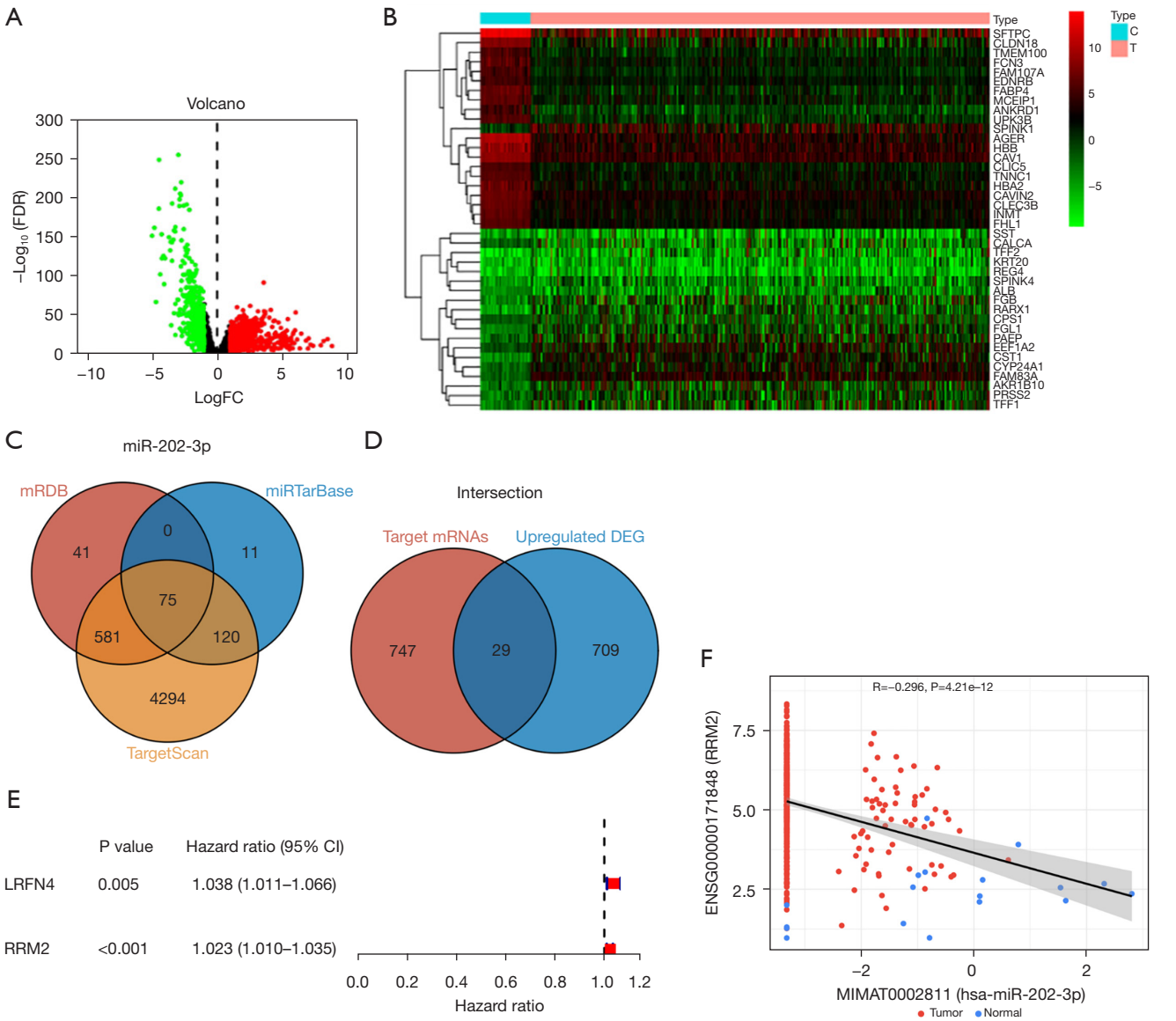

Figure 6 Prediction of *miR-202-3p* expression-related genes. (A) A volcano map of the DEGs associated with *miR-202-3p*. Red represents a significantly different and up-regulated gene; green represents a significant difference and down-regulation gene; genes with no significant difference in black. (B) Heatmap of DEGs between the high- and low-expression groups of DEGs (20 high-expression genes and 20 low-expression genes); red represents high expression; blue denotes low expression. (C) A Venn diagram shows the coexpressed genes in the mRDB, TargetScan, and miRTarBase databases. (D) A Venn diagram shows the coexpressed genes of the target gene and the upregulated DEGs. (E) Cox univariate proportional hazards regression analyses of *RRM2* and *LRFN4*. (F) CancerMIRNome analysis showed that the expression of *RRM2* and *miR-202-3p* in LUAD was negatively correlated. C, control; T, tumor; DEG, differentially expressed gene; FC, fold change; FDR, false discovery rate; LUAD, lung adenocarcinoma; *LRFN4*, leucine rich repeat and fibronectin type III domain containing 4; *RRM2*, ribonucleotide reductase regulatory subunit M2.

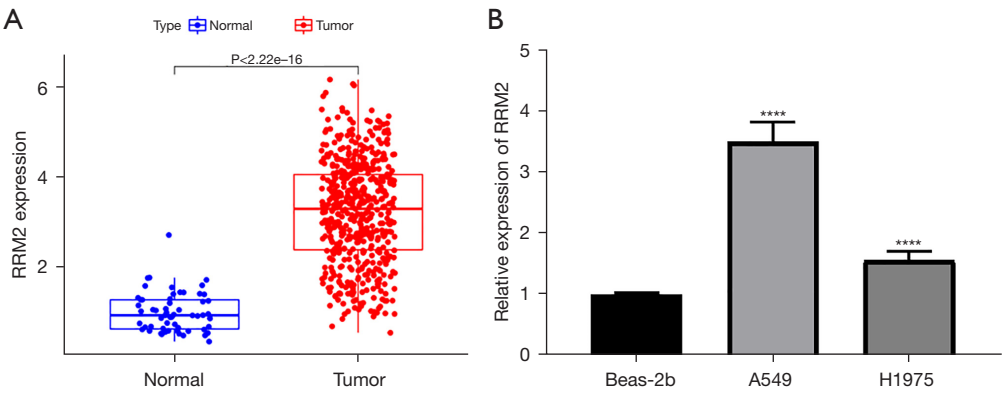

Figure 7 Expression of *RRM2* in LC cells. (A) In TCGA database, the expression of *RRM2* in tumors was higher than that in normal tissue (P<0.05). (B) The expression in A549 and H1975 cells was higher than that in Beas-2b cells. The P value was calculated using a parametric test: ****, P<0.0001. LC, lung cancer; *RRM2*, ribonucleotide reductase regulatory subunit M2; TCGA, The Cancer Genome Atlas.

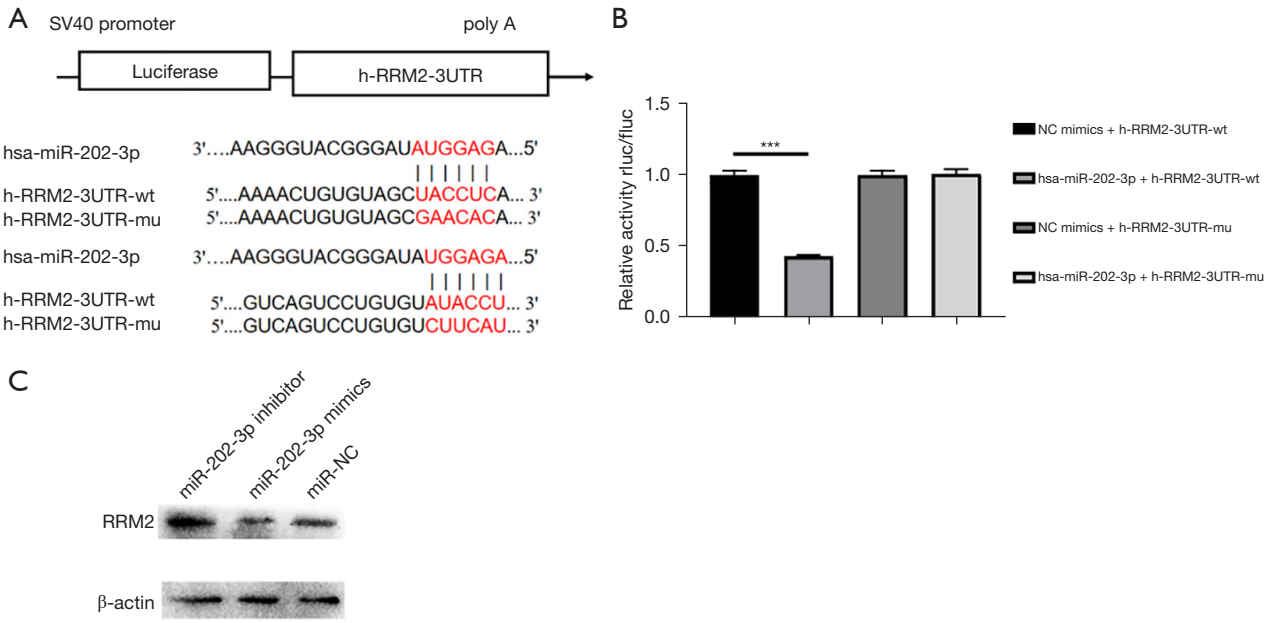

Figure 8 Luciferase reporter assay and Western blot. (A) Schematic diagram of the binding between the *hsa-miR-202-3p* and *h-RRM2-3UTR* target sites. (B) The interaction between *hsa-miR-202-3p* and *h-RRM2-3UTR* was detected by the dual luciferase reporter gene; the luciferase activity of the *hsa-miR-202-3p* + *h-RRM2-3UTR-wt* group was significantly reduced, with a P value of 1.13831e−05. (C) Western blot was used to detect the expression levels of the *RRM2* protein in each group after transfection. ***, P<0.001. NC, negative control; *RRM2*, ribonucleotide reductase regulatory subunit M2; 3UTR, 3' untranslated region; wt, wild type; mu, mutant; rluc/fluc, renilla luciferase/firefly luciferase.

Clinical correlation between RRM2 expression and LUAD

To better understand whether *RRM2* expression is related to the occurrence and development of LC, the correlation between *RRM2* expression and clinicopathological stage was further analyzed. From the perspective of tumor size and depth of invasion (T), the expression level of *RRM2* was the lowest in stage T1. Although the expression level of *RRM2* in stages T2 to T4 was T4 > T2 > T3, only the expression levels of *RRM2* in T1 and T2 were correlated with T stage (P<0.05); there were no other significant correlations (*Figure 9A*). From the perspective of lymph node metastasis (N), although N3 > N2 > N1 > N0, only N0 and N1 and

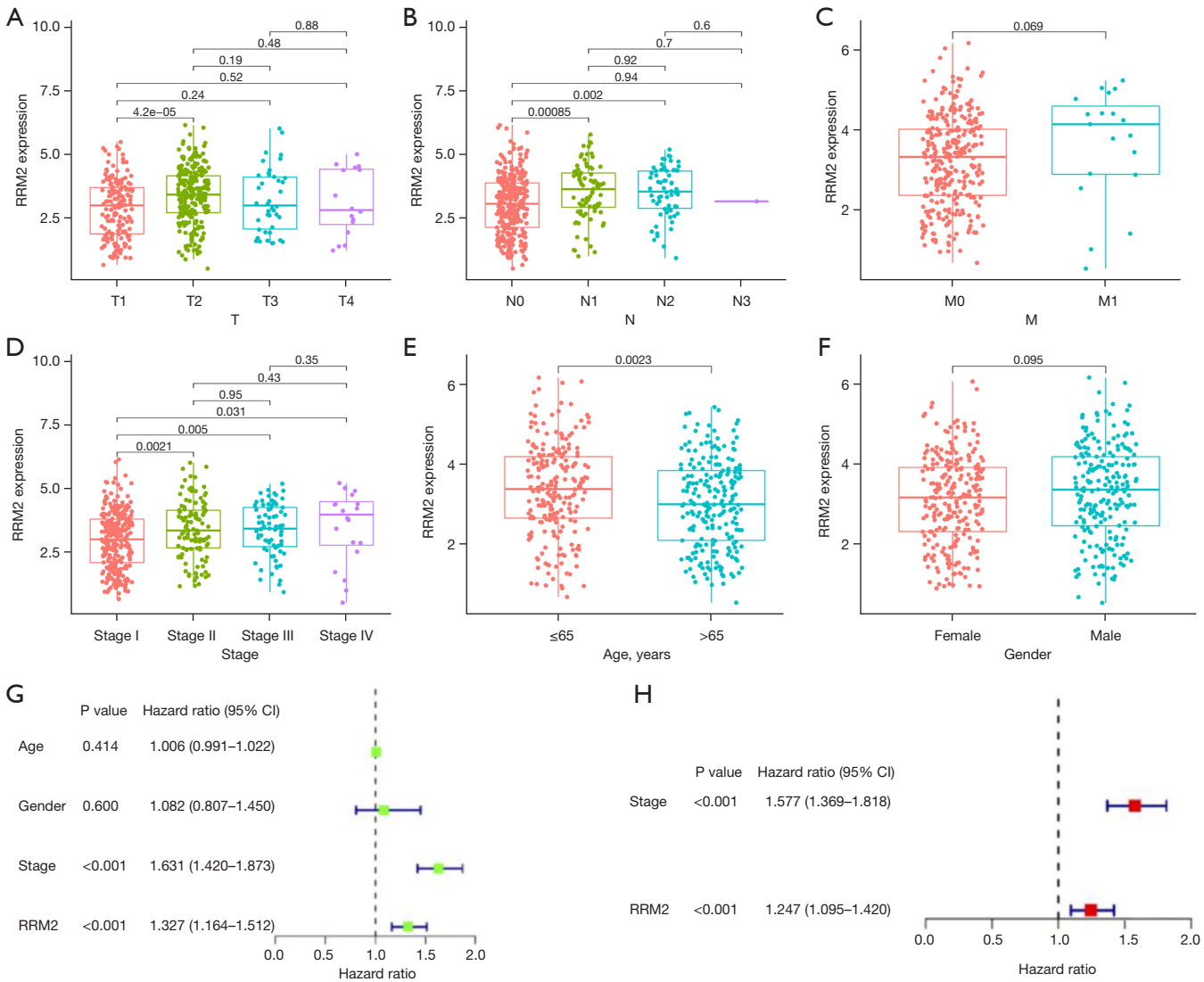

Figure 9 Correlation analysis between *RRM2* expression and clinical LC. (A) Correlation analysis between *RRM2* expression and T stage. The P values for stage T1 and stages T2, T3, and T4 were 4.2e–05, 0.24, and 0.52, respectively. (B) Correlation analysis of *RRM2* expression and N staging: the P values for N0 and N1, N2, and N3 were 0.00085, 0.002, and 0.94, respectively. (C) Correlation analysis between *RRM2* expression and M staging: the P value for M0 and M1 was 0.069. (D) Correlation analysis of *RRM2* expression and staging: the P values for stage I and stages II, III, and IV were 0.0021, 0.005, and 0.031, respectively. (E) Analysis of *RRM2* expression and age (>65- and ≤65-year groups). The expression of *RRM2* in the ≤65-year group was higher than that in the >65-year group, P<0.05. (F) Analysis of *RRM2* expression and sex. The *RRM2* expression level in males was higher than that in females, with a P value of 0.095. (G) Forest plot of the univariate Cox regression analysis of risk score and clinical characteristics. A significant P value indicates a relationship between characteristics and clinical prognosis. A hazard ratio greater than 1 indicates high-risk factors, and that less than 1 indicates low-risk factors; the 95% CI is in parentheses. (H) Forest plot of multivariate Cox regression analysis of risk score and clinical characteristics. A significant P value indicates a relationship between characteristics and clinical prognosis. A hazard ratio greater than 1 represents high-risk factors, and that less than 1 represents low-risk factors. CI, confidence interval; *RRM2*, ribonucleotide reductase regulatory subunit M2.

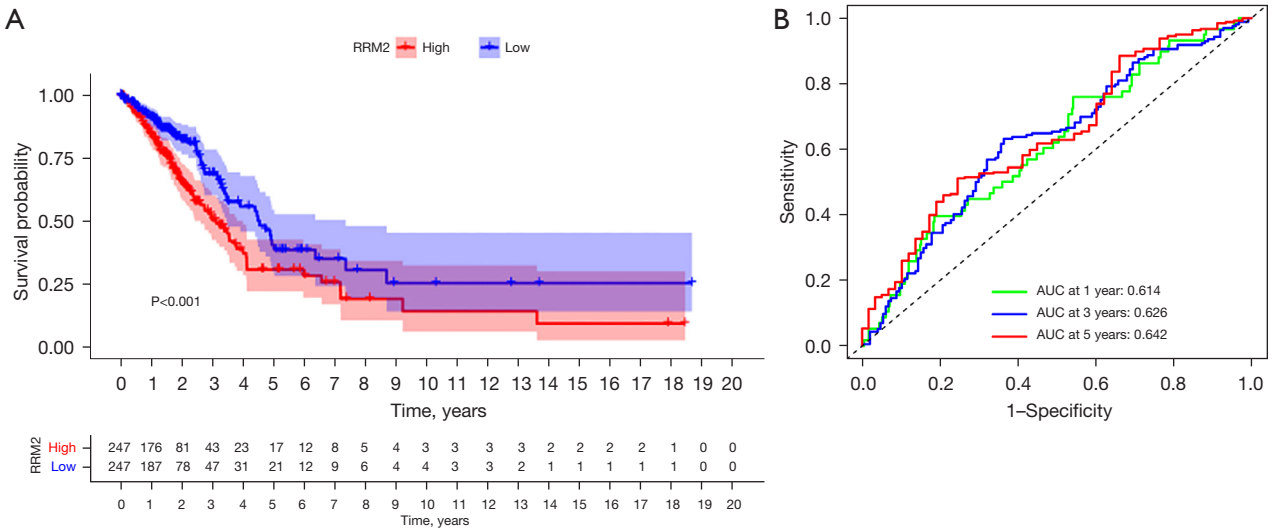

Figure 10 Survival analysis and ROC curves of *RRM2*. (A) The Kaplan-Meier survival curve indicated that low *RRM2* expression was associated with better overall prognosis (P<0.001). (B) ROC curve of *RRM2* expression. AUC, area under the curve; ROC, receiver operating characteristic; *RRM2*, ribonucleotide reductase regulatory subunit M2.

N0 and N2 were statistically correlated (P<0.05, *Figure 9B*). In terms of distant metastasis (M), the level of *RRM2* expression was higher for M1 than for M0 metastasis, i.e., the level of *RRM2* expression was correlated with distant metastasis (P=0.069), but this was not statistically significant (*Figure 9C*). Finally, for clinical stage, the level of *RRM2* expression was positively correlated with stage, and there was a significant difference between stage I and stages II, III, and IV (P<0.05, *Figure 9D*). The above data indicate that the level of *RRM2* expression is strongly correlated with TNM staging.

The correlation between *RRM2* expression level and age (>65 and ≤65 years) and sex was further analyzed. The results showed that the level of *RRM2* expression in patients aged ≤65 years was higher than that in patients aged >65 years, P<0.05 (*Figure 9E*). Also, the level of *RRM2* expression in males was higher than that in females, with a P value of 0.095, i.e., not significant (*Figure 9F*). Subsequently, univariate and multivariate Cox regression analyses were performed to further evaluate the performance of our model in LUAD patients and using other common prognostic factors. The univariate Cox analysis results showed that clinicopathological stage was closely related to the clinical survival prognosis of LUAD patients (*Figure 9G*). When these factors were included in the multivariate Cox analysis, only clinicopathological stage could be used as an independent risk factor for the prognosis of LUAD patients (*Figure 9H*).

Analysis of RRM2 expression and survival prognosis and ROC curve of LC patients

To explore the correlation between *RRM2* expression and survival, survival analysis was performed using RNA-seq data for LUAD in TCGA database and clinical data for LUAD patients downloaded from the UCSC (University of California Santa Cruz) XENA database. The K-M survival curve showed that the survival rate of the *RRM2* high-expression group was lower than that of the *RRM2* low-expression group (P<0.05, *Figure 10A*). To verify the diagnostic value of *RRM2*, we generated a ROC curve for patient *RRM2* expression levels; the AUCs at 1, 3, and 5 years were 0.614, 0626, and 0.642, respectively (*Figure 10B*), indicating that *RRM2* has a strong diagnostic effect in LC.

KEGG enrichment analysis of RRM2

To further understand the role of the *RRM2* protein in cellular metabolic activities and the molecular functions, biological processes, and signaling pathways involved, KEGG pathway enrichment analysis was performed for *RRM2* using the clusterProfiler software package in R language. KEGG analysis revealed *RRM2* enrichment in the Notch pathway (*Figure 11*).

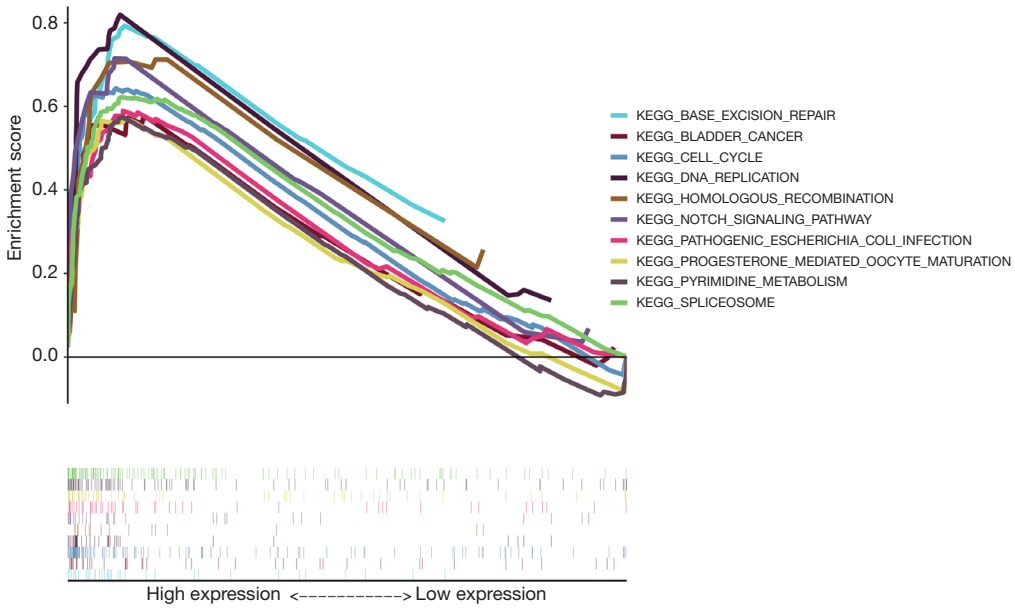

Figure 11 KEGG analysis of *RRM2*. KEGG analysis revealed *RRM2* might play a role through the Notch pathway. KEGG, Kyoto Encyclopedia of Genes and Genomes; *RRM2*, ribonucleotide reductase regulatory subunit M2.

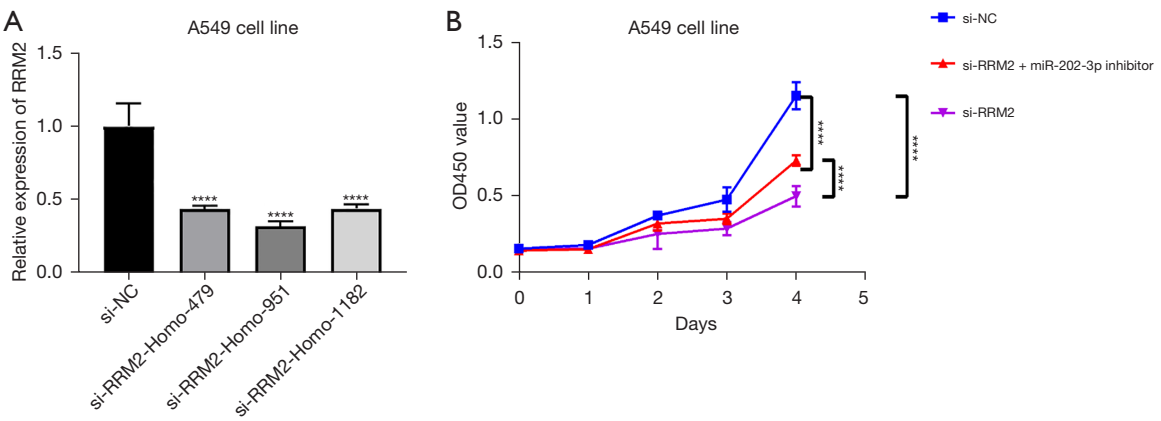

Figure 12 *RRM2* inhibits the migration and invasion of A549 cells. (A) The expression of *RRM2* in A549 cells after transfection of si-NC, si-*RRM2-Homo-479*, si-*RRM2-Homo-951*, and si-*RRM2-Homo-1182*; the P value was calculated using a parametric test: ****, P<0.0001. (B) CCK-8 assay for A549 cells in the si-*RRM2* group, si-*RRM2* + *miR-202-3p* inhibitor group, and si-NC group. The growth rate of A549 cells in the si-*RRM2* group was the slowest, followed by those in the si-*RRM2* + *miR-202-3p* inhibitor group and the si-NC group, which exhibited the fastest growth. The P value was calculated using a parametric test: ****, P<0.0001. CCK-8, Cell Counting Kit 8; NC, negative control; OD, optical density; *RRM2*, ribonucleotide reductase regulatory subunit M2.

RRM2 promotes the proliferation of LUAD cells

Following transfection of A549 cells with si-*RRM2-Homo-479*, si-*RRM2-Homo-951*, and si-*RRM2-Homo-1182*, the expression of *RRM2* in the above three siRNA groups was lower than that in the si-NC group (P<0.05, *Figure 12A*). Si-*RRM2-Homo-951* led to the greatest decrease in *RRM2* and was thus used in subsequent experiments. The growth rate of A549 cells in the si-*RRM2* group was slower than that of A549 cells in the si-NC group and the si-*RRM2* + *miR-202-3p* inhibitor group. Also, the growth rate of A549 cells in the si-*RRM2* + *miR-202-3p* inhibitor group was slower than

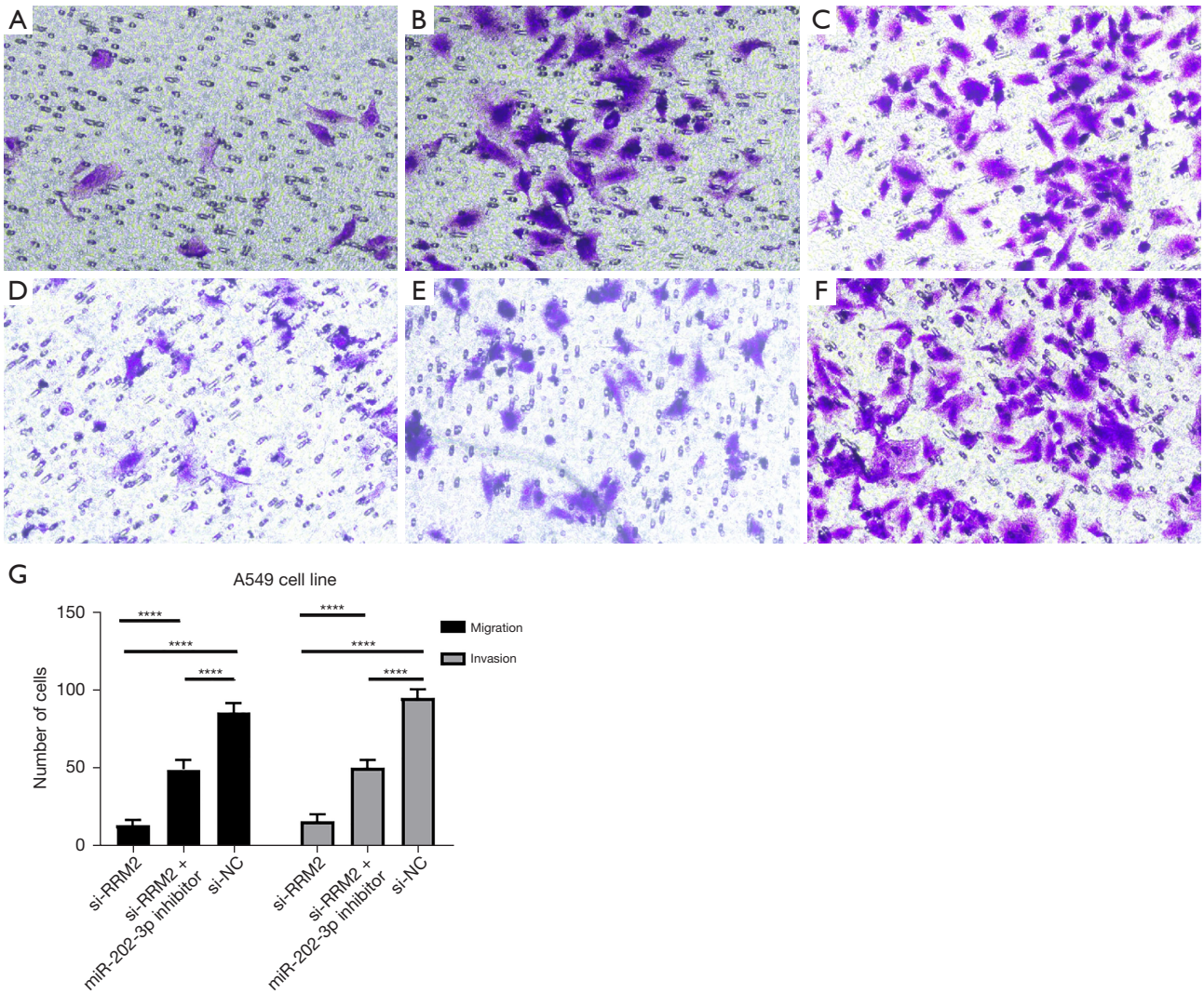

Figure 13 Transwell assay of the migration and invasion ability of each group of cells (crystal violet staining). (A) Migration of A549 cells in the si-*RRM2* group; (B) migration of A549 cells in the si-*RRM2* + *miR-202-3p* inhibitor group; (C) migration of A549 cells in the si-NC group; (D) invasion of A549 cells in the si-*RRM2* group; (E) invasion of A549 cells in the si-*RRM2* + *miR-202-3p* inhibitor group; (F) invasion of A549 cells in the si-NC group; (G) the number of migrating and invading cells; intergroup comparisons were conducted. The P value was calculated using a parametric test: ****, P<0.0001. NC, negative control; *RRM2*, ribonucleotide reductase regulatory subunit M2. Original magnification was ×200 for A-F.

that of A549 cells in the si-NC group but faster than that of A549 cells in the si-*RRM2* group, indicating that *RRM2* promoted the proliferation of A549 cells and that the *miR-202-3p* inhibitor reduced the inhibitory effect of si-*RRM2* on the growth of A549 cells (*Figure 12B*).

RRM2 promotes the migration and invasion of LUAD cells

Transwell assays were applied to assess the migration and invasion of LUAD cells in the si-*RRM2* group, the *miR-202-3p* inhibitor + si-*RRM2* group, and the si-NC group. The si-NC group had the most cells pass through the Transwell, followed by the *miR-202-3p* inhibitor + si-*RRM2* group and the si-*RRM2* group, which had the fewest number of cells pass through the Transwell. All P values were less than 0.05 in the intergroup comparisons (*Figure 13*). This finding indicates that *RRM2* promotes the invasion and metastasis of A549 cells.

Previous experiments have shown that *miR-202-3p* directly targets *RRM2*; furthermore, the number of migrating and invading cells in the *miR-202-3p* inhibitor group was higher than that in the si-*RRM2* group but less than the si-NC group, indicating that the *miR-202-3p* inhibitor alleviated the inhibitory effect of si-*RRM2* on *RRM2*, further demonstrating the direct targeting effect of *miR-202-3p* on *RRM2*.

Discussion

In recent decades, the incidence of LC has increased significantly due to air pollution and other factors, of which the increase in the incidence of NSCLC has been the most significant (25,26). Although a large proportion of NSCLC patients are diagnosed early and receive treatment, the overall prognosis of LC patients is very poor due to frequent recurrence and metastasis (27).

MiRNAs are small non-coding RNAs that act as posttranscriptional mediators of gene expression through the silencing or degradation of mRNAs (messenger RNAs). In recent years, numerous studies have been conducted on miRNAs, and there is a considerable amount of evidence showing that there are many connections between miRNAs and the occurrence and development of tumors. The occurrence and development of several cancers are closely related to the dysregulation of miRNAs. MiRNAs act as tumor suppressors or oncogenes (oncomiRs), and miRNA mimics and miRNA targeting molecules (antimiRs) have shown promise in preclinical development (28). Recently, a previous study has demonstrated that miRNAs can regulate the development of a variety of tumors and have important effects on tumor development, prognosis, and treatment (29). MiRNAs inhibit different target genes to affect the proliferation, migration, and invasion of cancer cells. For example, the overexpression of *miR-25-3p* inhibits regulator of G-protein signaling (RGS3). Also, the inhibition of *miR-25* promotes the apoptosis and delays the proliferation of NSCLC cells (30). *MiR-125b* can promote tumor metastasis in human NSCLC cells by targeting tumor protein 53-induced nuclear protein 1 (*TP53INP1*) (31). Additionally, miR-31 overexpression may be associated with cisplatin (DDP) resistance, and miR-31 can exert an anti-apoptotic effect by inhibiting the 3'UTR of ABC transporter 9 protein (ABCB9), which is a key factor in the mediation of DDP resistance (32). *MiR-31* may also promote the development of LC by stimulating mutant Kirsten rat sarcoma viral oncogene homolog (*KRAS*) (33). In summary, the identification of miRNAs and their target genes and pathways associated with NSCLC can be used as an entry point to develop treatments for LC, which is a highly malignant tumor in clinical practice.

There is evidence that *miR-202-3p* is associated with a variety of human diseases. For example, the silencing of *miR-202-3p* in metastatic breast cancer can promote the expression of matrix metalloproteinase 1 (MMP-1) and an infiltrating phenotype in brain cells (34); *miR-202-3p* can target brain-derived neurotrophic factors and participate in depression-like behaviors (35). *MiRNA-202-3p* can also target transient receptor potential cation channel, subfamily M, member 6 (TRPM6) and protect the heart from myocardial ischemia-reperfusion injury by activating TGF-cads1/Smad signaling (36). However, the mechanism by which *miR-202-3p* promotes LC metastasis and proliferation in NSCLC is still unknown.

In this study, the expression of *miR-203-3p* in NSCLC tissue and cells was significantly lower than that in adjacent tissue and normal lung cells. Subsequently, we validated this hypothesis using data analysis and qPCR experiments. We focused on elucidating the potential mechanism of *miR-202-3p*-mediated promotion of LUAD metastasis. We observed that the expression level of *miR-202-3p* was significantly decreased in NSCLC tissue and cells, while its overexpression inhibited the proliferation and migration of tumor cells *in vitro*. The TargetScan data analysis conducted in this study also showed that *RRM2* might directly interact with *miR-202-3p*. In other words, *miR-202-3p* might target and regulate *RRM2*. To verify this hypothesis, we performed a dual luciferase reporter gene analysis, and the results indicated that *miR-202-3p* could directly target *RRM2*.

The full name of *RRM2* is ribonucleoside reductase M2, which is a subunit of RR. RR is the only enzyme that can catalyze the *de novo* formation of deoxyribonucleoside and is critical in DNA synthesis. High *RRM2* expression is very common in cancer, and *RRM2* is considered to be a promoting factor and therapeutic target for the occurrence and development of tumors (37). Numerous studies have shown that *RRM2* expression is related to the activity of chemotherapeutic drugs in cancer (37-39). High *RRM2* expression is associated with low sensitivity to chemotherapy and poor prognosis (40). Using multi-omics and bioinformatics analysis, *RRM2* upregulation was shown to be associated with chemotherapy resistance and poor prognosis; however, these results need to be verified in *in vivo* and *in vitro* experiments and multicenter randomized controlled clinical trials (41). The upregulation

of *RRM2* affects complex signaling pathways and mediates the survival, proliferation, migration, invasion, and chemotherapy resistance of cancer cells. Therefore, *RRM2* may be a potential target for overcoming chemotherapy resistance. *RRM2* not only has broad application prospects in chemotherapy but also has clinical significance in terms of cancer diagnosis and the prediction of patient prognosis, as verified by numerous studies. For example, high *RRM2* expression in LC can be used as an independent predictor of poor prognosis (42).

In terms of mechanism, *miR-202-3p* inhibited *RRM2*-mediated proliferation and invasion of NSCLC cells by inhibiting *RRM2*. These results suggest that *miR-202-3p* may be a therapeutic molecule for the clinical treatment of NSCLC, a dangerous malignant tumor.

Through data analysis carried out in this study, we found that *RRM2* expression was low in paracancerous tissue and high in cancer tissue. An analysis of TCGA data and qPCR of normal lung epithelial cells and lung SCLC cells confirmed the high expression of *RRM2* in LC tissue. Moreover, the CCK-8 and Transwell assays performed in this study demonstrated that *RRM2* promoted the proliferation and metastasis of LC cells. In the co-transfection experiment with a *miR-202-3p* inhibitor and si-*RRM2*, the results showed that the proliferation and metastasis of cells in the transfection group were faster than those of cells in the si-*RRM2* group but slower than those of cells in the si-NC group, confirming that *miR-202-3p* and *RRM2* have a targeted effect. High *RRM2* expression is common in cancer.

We also found that the overexpression of *miR-202-3p* inhibited the proliferation and metastasis of LUAD. MiRNAs play a gene regulatory role by binding to the 3'UTR of target mRNA. We identified the enrichment of *RRM2* in the Notch pathway. Notch signaling regulates a variety of cell fate decisions in multiple tissues, including lineage commitment, differentiation, cell cycle progression, as well as stem cell maintenance and self-renewal (43,44). Studies on the role of Notch signaling in tumorigenesis have mainly focused on the role of Notch as an oncogene; Notch is considered to be an oncogene in several cancers, including brain cancer, breast cancer, ovarian cancer, and NSCLC (45-47). These findings can provide some ideas for further research on *RRM2*. In recent years, gene transfection has been widely used to regulate gene expression. These findings can provide new ideas and directions for the treatment of LUAD.

In summary, our study showed that the expression of *miR-202-3p* was downregulated in NSCLC tumor tissue and LUAD cells and that the expression of *RRM2* was upregulated. In addition, we also demonstrated the direct-targeted regulation of *miR-202-3p* and *RRM2* and demonstrated that *miR-202-3p* inhibited the proliferation and metastasis of LUAD through the targeted inhibition of *RRM2*. Furthermore, there was a correlation between the *RRM2* expression level and clinical characteristics, demonstrating that *RRM2* has a certain value in predicting the prognosis of and diagnosing LUAD. These findings provide effective molecular targets for the treatment of LUAD.

Conclusions

In this study, LUAD RNA-seq data from TCGA were used as subjects, and the genes targeted by *miR-202-3p* were identified through serial analysis. Next, *miR-202-3p* and the targeted gene, *RRM2*, were validated. Furthermore, the roles of *miR-202-3p* and *RRM2* in LC cells were explored. The pathology and prognosis of *RRM2* in LC patients were also evaluated through data analysis. The main conclusions were as follows: (I) *msiR-202-3p* is lowly expressed in LC tissue, and *miR-202-3p* overexpression inhibits the proliferation and metastasis of LC cells; (II) *RRM2* is highly expressed in LC tissue and promotes the proliferation and metastasis of LC cells; (III) *miR-202-3p* inhibits *RRM2*, thereby reducing the proliferation and metastasis of LUAD cells; and (IV) the prognosis of LUAD patients with low *RRM2* expression is good, and the level of *RRM2* expression is correlated with the clinical characteristics of LC patients.

Acknowledgments

Funding: This work was supported by Natural Science Research Project of Nantong Science and Technology Bureau (No. MS12020029).

Footnote

Reporting Checklist: The authors have completed the MDAR reporting checklist. Available at https://atm.amegroups.com/article/view/10.21037/atm-22-6089/rc

Data Sharing Statement: Available at https://atm.amegroups.com/article/view/10.21037/atm-22-6089/dss

Conflicts of Interest: All authors have completed the

ICMJE uniform disclosure form (available at https://atm.amegroups.com/article/view/10.21037/atm-22-6089/coif). The authors have no conflicts of interest to declare.

Ethical Statement: The authors are accountable for all aspects of the work in ensuring that questions related to the accuracy or integrity of any part of the work are appropriately investigated and resolved. The study was conducted in accordance with the Declaration of Helsinki (as revised in 2013).

References

1. Bray F, Ferlay J, Soerjomataram I, et al. Global cancer statistics 2018: GLOBOCAN estimates of incidence and mortality worldwide for 36 cancers in 185 countries. CA Cancer J Clin 2018;68:394-424.
2. Liu D. CAR-T "the living drugs", immune checkpoint inhibitors, and precision medicine: a new era of cancer therapy. J Hematol Oncol 2019;12:113.
3. Wang S, Zimmermann S, Parikh K, et al. Current Diagnosis and Management of Small-Cell Lung Cancer. Mayo Clin Proc 2019;94:1599-622.
4. Meza R, Meernik C, Jeon J, et al. Lung cancer incidence trends by gender, race and histology in the United States, 1973-2010. PLoS One 2015;10:e0121323.
5. Zhang C, Yin K, Liu SY, et al. Multiomics analysis reveals a distinct response mechanism in multiple primary lung adenocarcinoma after neoadjuvant immunotherapy. J Immunother Cancer 2021;9:e002312.
6. Noma D, Inamura K, Matsuura Y, et al. ALK-rearranged lung adenocarcinoma showing intra-bronchial protrusion: a case of actually peripheral origin with a rare spreading pattern. Ann Clin Oncol 2017;1:15.
7. Zhao Y, Brasier AR. Uronic acid pathway metabolites regulate mesenchymal transition and invasiveness in lung adenocarcinoma. Biotarget 2019;3:19.
8. Kabekkodu SP, Shukla V, Varghese VK, et al. Clustered miRNAs and their role in biological functions and diseases. Biol Rev Camb Philos Soc 2018;93:1955-86.
9. Ali Syeda Z, Langden SSS, Munkhzul C, et al. Regulatory Mechanism of MicroRNA Expression in Cancer. Int J Mol Sci 2020;21:1723.
10. Hill M, Tran N. miRNA interplay: mechanisms and consequences in cancer. Dis Model Mech 2021;14:dmm047662.
11. Dou D, Li XK, Xia QS, et al. Circulating miRNA-202-3p is a potential novel biomarker for diagnosis of type 1 gastric neuroendocrine neoplasms. BMC Gastroenterol 2021;21:188.
12. Yu G, Sun W, Wang W, et al. Overexpression of microRNA-202-3p in bone marrow mesenchymal stem cells improves cerebral ischemia-reperfusion injury by promoting angiogenesis and inhibiting inflammation. Aging (Albany NY) 2021;13:11877-88.
13. Xu C, Zhai J, Fu Y. Overexpression of Nuclear Enriched Autosomal Transcript 1 Facilitates Cell Proliferation, Migration Invasion, and Suppresses Apoptosis in Endometrial Cancer by Targeting MicroRNA-202-3p/T Cell Immunoglobulin and Mucin Domain 4 Axis. Cancer Biother Radiopharm 2022;37:815-23.
14. Lamb NA, Bard JE, Loll-Krippleber R, et al. Complex mutation profiles in mismatch repair and ribonucleotide reductase mutants reveal novel repair substrate specificity of MutS homolog (MSH) complexes. Genetics 2022;221:iyac092.
15. Wu Z, Zhan Y, Wang L, et al. Identification of osalmid metabolic profile and active metabolites with anti-tumor activity in human hepatocellular carcinoma cells. Biomed Pharmacother 2020;130:110556.
16. Wang N, Zhan T, Ke T, et al. Increased expression of RRM2 by human papillomavirus E7 oncoprotein promotes angiogenesis in cervical cancer. Br J Cancer 2014;110:1034-44.
17. Duxbury MS, Whang EE. RRM2 induces NF-kappaB-dependent MMP-9 activation and enhances cellular invasiveness. Biochem Biophys Res Commun 2007;354:190-6.
18. Rasmussen RD, Gajjar MK, Tuckova L, et al. Author Correction: BRCA1-regulated RRM2 expression protects glioblastoma cells from endogenous replication stress and promotes tumorigenicity. Nat Commun 2018;9:5396.
19. Wang M, Chen X, Jin W, et al. Ginsenoside Rb3 exerts protective properties against cigarette smoke extract-

induced cell injury by inhibiting the p38 MAPK/NF-κB and TGF-β1/VEGF pathways in fibroblasts and epithelial cells. Biomed Pharmacother 2018;108:1751-8.
20. Rahman MA, Amin AR, Wang D, et al. RRM2 regulates Bcl-2 in head and neck and lung cancers: a potential target for cancer therapy. Clin Cancer Res 2013;19:3416-28.
21. Xia G, Wang H, Song Z, et al. Gambogic acid sensitizes gemcitabine efficacy in pancreatic cancer by reducing the expression of ribonucleotide reductase subunit-M2 (RRM2). J Exp Clin Cancer Res 2017;36:107.
22. Kałuzińska Ż, Kołat D, Bednarek AK, et al. PLEK2, RRM2, GCSH: A Novel WWOX-Dependent Biomarker Triad of Glioblastoma at the Crossroads of Cytoskeleton Reorganization and Metabolism Alterations. Cancers (Basel) 2021;13:2955.
23. Liu Q, Guo L, Qi H, et al. A MYBL2 complex for RRM2 transactivation and the synthetic effect of MYBL2 knockdown with WEE1 inhibition against colorectal cancer. Cell Death Dis 2021;12:683.
24. Ma C, Luo H, Cao J, et al. Independent prognostic implications of RRM2 in lung adenocarcinoma. J Cancer 2020;11:7009-22.
25. Urman A, Dean Hosgood H. Lung Cancer Risk, Genetic Variation, and Air Pollution. EBioMedicine 2015;2:491-2.
26. Ganti AK, Klein AB, Cotarla I, et al. Update of Incidence, Prevalence, Survival, and Initial Treatment in Patients With Non-Small Cell Lung Cancer in the US. JAMA Oncol 2021;7:1824-32.
27. Schanne DH, Heitmann J, Guckenberger M, et al. Evolution of treatment strategies for oligometastatic NSCLC patients - A systematic review of the literature. Cancer Treat Rev 2019;80:101892.
28. Rupaimoole R, Slack FJ. MicroRNA therapeutics: towards a new era for the management of cancer and other diseases. Nat Rev Drug Discov 2017;16:203-22.
29. Goodall GJ, Wickramasinghe VO. RNA in cancer. Nat Rev Cancer 2021;21:22-36.
30. Chen Z, Wu Y, Meng Q, et al. Elevated microRNA-25 inhibits cell apoptosis in lung cancer by targeting RGS3. In Vitro Cell Dev Biol Anim 2016;52:62-7.
31. Li Q, Han Y, Wang C, et al. MicroRNA-125b promotes tumor metastasis through targeting tumor protein 53-induced nuclear protein 1 in patients with non-small-cell lung cancer. Cancer Cell Int 2015;15:84.
32. Dong Z, Zhong Z, Yang L, et al. MicroRNA-31 inhibits cisplatin-induced apoptosis in non-small cell lung cancer cells by regulating the drug transporter ABCB9. Cancer Lett 2014;343:249-57.
33. Edmonds MD, Boyd KL, Moyo T, et al. MicroRNA-31 initiates lung tumorigenesis and promotes mutant KRAS-driven lung cancer. J Clin Invest 2016;126:349-64.
34. Harati R, Hafezi S, Mabondzo A, et al. Silencing miR-202-3p increases MMP-1 and promotes a brain invasive phenotype in metastatic breast cancer cells. PLoS One 2020;15:e0239292.
35. Zhou B, Zhu H, Luo H, et al. MicroRNA-202-3p regulates scleroderma fibrosis by targeting matrix metalloproteinase 1. Biomed Pharmacother 2017;87:412-8.
36. Wu HY, Wu JL, Ni ZL. Overexpression of microRNA-202-3p protects against myocardial ischemia-reperfusion injury through activation of TGF-β1/Smads signaling pathway by targeting TRPM6. Cell Cycle 2019;18:621-37.
37. Aye Y, Li M, Long MJ, et al. Ribonucleotide reductase and cancer: biological mechanisms and targeted therapies. Oncogene 2015;34:2011-21.
38. Ding J, Li F, Cong Y, et al. Trichostatin A inhibits skeletal muscle atrophy induced by cigarette smoke exposure in mice. Life Sci 2019;235:116800.
39. Zhou S, Li J, Xu H, et al. Liposomal curcumin alters chemosensitivity of breast cancer cells to Adriamycin via regulating microRNA expression. Gene 2017;622:1-12.
40. Mao G, Li L, Shan C, et al. High expression of RRM2 mediated by non-coding RNAs correlates with poor prognosis and tumor immune infiltration of hepatocellular carcinoma. Front Med (Lausanne) 2022;9:833301.
41. Liu R, Guo CX, Zhou HH. Network-based approach to identify prognostic biomarkers for estrogen receptor-positive breast cancer treatment with tamoxifen. Cancer Biol Ther 2015;16:317-24.
42. Jin CY, Du L, Nuerlan AH, et al. High expression of RRM2 as an independent predictive factor of poor prognosis in patients with lung adenocarcinoma. Aging (Albany NY) 2020;13:3518-35.
43. Cai H, Guo H, Deng Y, et al. RRM2 regulates osteogenesis of mouse embryo fibroblasts via the Wnt/β-catenin signaling pathway. Exp Ther Med 2022;24:605.
44. Li C, Zheng J, Chen S, et al. RRM2 promotes the progression of human glioblastoma. J Cell Physiol 2018;233:6759-67.
45. Teodorczyk M, Schmidt MHH. Notching on Cancer's Door: Notch Signaling in Brain Tumors. Front Oncol 2014;4:341.
46. Zhou B, Lin W, Long Y, et al. Notch signaling pathway:

architecture, disease, and therapeutics. Signal Transduct Target Ther 2022;7:95.
47. Ferreira A, Aster JC. Notch signaling in cancer: Complexity and challenges on the path to clinical translation. Semin Cancer Biol 2022;85:95-106.

Cite this article as: Cao X, Xue F, Chen H, Shen L, Yuan X, Yu Y, Zong Y, Zhong L, Huang F. MiR-202-3p inhibits the proliferation and metastasis of lung adenocarcinoma cells by targeting RRM2. Ann Transl Med 2022;10(24):1374. doi: 10.21037/atm-22-6089

